AGU PUBLICATIONS

JGR

Journal of Geophysical Research: Oceans

RESEARCH ARTICLE

10.1002/2015JC011536

Key Points:
- Measuring swell attenuation and dissipation using altimeter data and model output
- Giving an acceptance range and a recommended value of swell dissipation rate
- Discussing the roles of dispersion, angular spreading and dissipation in swell height attenuation

Correspondence to:
G. Chen,
gechen@ouc.edu.cn

Citation:
Jiang, H., J. E. Stopa, H. Wang, R. Husson, A. Mouche, B. Chapron, and G. Chen (2016), Tracking the attenuation and nonbreaking dissipation of swells using altimeters, *J. Geophys. Res. Oceans*, *121*, 1446–1458, doi:10.1002/2015JC011536.

Received 8 DEC 2015
Accepted 14 JAN 2016
Accepted article online 19 JAN 2016
Published online 20 FEB 2016

Tracking the attenuation and nonbreaking dissipation of swells using altimeters

Haoyu Jiang[1,2], Justin E. Stopa[2], He Wang[2,3], Romain Husson[4], Alexis Mouche[2], Bertrand Chapron[2], and Ge Chen[1]

[1]Qingdao Collaborative Innovation Center of Marine Science and Technology, College of Information Science and Engineering, Ocean University of China, Qingdao, China, [2]Laboratoire d'Océanographie Spatiale, Centre de Brest, IFREMER, Plouzané, France, [3]National Ocean Technology Center, State Oceanic Administration, Tianjin, China, [4]Collecte Localisation Satellites, Plouzané, France

Abstract A method for systematically tracking swells across oceanic basins is developed by taking advantage of high-quality data from space-borne altimeters and wave model output. The evolution of swells is observed over large distances based on 202 swell events with periods ranging from 12 to 18 s. An empirical attenuation rate of swell energy of about 4×10^{-7} m^{-1} is estimated using these observations, and the nonbreaking energy dissipation rates of swells far away from their generating areas are also estimated using a point source model. The resulting acceptance range of nonbreaking dissipation rates is -2.5 to 5.0×10^{-7} m^{-1}, which corresponds to a dissipation e-folding scales of at least 2000 km for steep swells, to almost infinite for small-amplitude swells. These resulting rates are consistent with previous studies using in-situ and synthetic aperture radar (SAR) observations. The frequency dispersion and angular spreading effects during swell propagation are discussed by comparing the results with other studies, demonstrating that they are the two dominant processes for swell height attenuation, especially in the near field. The resulting dissipation rates from these observations can be used as a reference for ocean engineering and wave modeling, and for related studies such as air-sea and wind-wave-turbulence interactions.

1. Introduction

Ocean swell is typically regarded as waves that hardly affected by the local wind. As the phase speed cannot exceed 1.2 times the sea surface wind speed at 10 m height during the development of waves, long swells are usually generated by intense wind [*Pierson and Moskowitz*, 1964]. An important source of ocean swells is the strong storms over the ocean, which can produce long surface gravity waves and "radiate" them out of their generating area [*Collard et al*., 2009]. Long-period swells are observed to be able to propagate over large distances, radiating momentum and energy across ocean basins [e.g., *Munk et al*., 1963; *Collard et al*., 2009].

When wind-waves are generated, nonlinear interaction transfers energy from high frequency to low frequency and turns the waves into swells. During the propagation of swell, its evolution may be affected by many local features such as the wind, other wave systems, currents, topography, mutual wave-wave interaction, etc. However, many of them can be ignored under certain circumstances. For example, nonlinear wave-wave interactions are often considered as a negligible term as swells propagate away from their source areas [*Hasselmann*, 1963], and the turbulence in the ocean also does not appear to significantly affect the swell propagation track [*Ardhuin and Jenkins*, 2006]. Generally, swells far from their generating areas are expected to be consistent over large distances with a constant period and group speed along the great circles on the Earth surface in deep oceans away from islands and in the absence of currents [*Snodgrass et al*., 1966; *Collard et al*., 2009].

The wave height of the long swells usually decreases during the process of propagation. Generally, the attenuation of swell wave height can be attributed to two categories of processes: The first category is the redistribution of energy in the same wave system, and the second one is the loss of energy. The representative phenomena of the first category include frequency dispersion and angular spreading effect, during which the total energy is conservative for the whole swell field. For example, in the process of frequency dispersion, the wave trains extending during propagation due to different group speeds leads to the

decrease of energy density in a unit area in the swell field. However, the total energy of the swell field remains conserved. The second category includes processes such as swell dissipating the energy into turbulence [*Ardhuin et al*., 2009; *Babanin*, 2012] and friction loss due to the seafloor in the shallow waters. In the processes of the second category, the wave height is attenuated because the swells transfer the wave energy to other mediums or processes.

The total attenuation rate of long swells in deep water should be small considering the fact that many swells generated in the Southern Ocean can propagate across the whole Pacific before reaching the coast of Alaska [*Snodgrass et al*., 1966]. Among the factors of attenuation of swells at large distances from their sources, frequency dispersion and angular spreading are often regarded as the first leading order. Another potential factor that significantly decreases the wave height of swell is the nonbreaking dissipation. Many studies highlighted its importance because of its impacts in numerical of wave models [e.g., *Ardhuin et al*., 2010; *Zieger et al*., 2015], studies of air-sea interaction [e.g., *Grachev and Fairall*, 2001; *Högström et al*., 2013] and wave-current-turbulence interaction [e.g., *Babanin*, 2006, 2012].

In spite of importance, there is not much quantitative information, especially field experiments, on the swell evolution over large distances. Laboratory studies and numerical experiments present and test some potential mechanisms for swell dissipation [e.g., *Babanin and Haus*, 2009; *Perignon et al*., 2014]. Some studies of air-sea interactions also demonstrate that swells can transfer momentum into the lower atmosphere [e.g., *Semedo et al*., 2009; *Högström et al*., 2013]. However, very few studies of field experiments, have been conducted to investigate the attenuation and dissipation of swells [*Snodgrass et al*., 1966; *Ardhuin et al*., 2009; *Young et al*., 2013]. In these three studies, the swells are measured using different instruments and methods. *Snodgrass et al*. [1966] arranged a sensor array along a great circle in the Pacific to trace the swell evolution at oceanic scales and used these in situ measurements to estimate the rate of swell dissipation. Some shortcomings do exist in their method: swells rarely propagate along the measurement array and the island sheltering effect introduces some errors. However, using these data, they gave a quantitative description of swell dissipation for the first time in history. *Collard et al*. [2009] develop a method of tracking deep water swells using the wave mode of Synthetic Aperture Radar (SAR), and with this method *Ardhuin et al*. [2009] present a range of swell dissipation rates based on 22 swell events, which marks the first application of remote sensing in this topic. *Young et al*. [2013] select significant wave height (SWH) from altimeter data in conditions of low winds (< 10 m s^{-1}) and swell direction being along the altimeter track. Only from the data in the Great Australian Bight, they capture a lot more swell events than previous studies. However, they neglect the frequency dispersion and the angular spread effects and result in a decay rate corresponding to an e-folding scale of less than 800 km, falling out of a reasonable range.

Although *Young et al*. [2013] did not adequately remove effects from frequency dispersion and angular spreading, they did provide a very inspiring method of measuring swell dissipation combining altimeter data and model output. Wave data measured from altimeters have proved its importance to global wave studies [*Young et al*., 2011], model verification [*Ardhuin et al*., 2010], and even the global swell field [*Chen et al*., 2002; *Jiang and Chen*, 2013]. Recently, a physical model of measuring wave period from altimeter data is presented by *Badulin* [2014], showing more potential of the altimeter in wave studies. Compared to SAR data, the altimeter has some unique advantages in this topic. First, the altimeter-measured SWH is more accurate and more precise than the swell SWH derived from SAR data [*Queffeulou et al*., 2011; *Wang et al*., 2014]. Second, the along-track sampling density of altimeter (about one measurement every 7 km) is higher than that of the SAR wave mode (about one image every 100 km), which can equate to a better statistical significance. Third, there are at least three altimeters in operation concurrently since 1995, offering a more expansive data set. Therefore, altimeter data can provide the critical information of SWHs to measure the decay, while the models such as WAVEWATCH IIIR (hereinafter WW3) [*Tolman and The WAVEWATCH III® Development Group*, 2014] can provide supplementary information of wave directions and wave periods to trace swells. The altimeter is a potential tool to observe and analyze the swell evolution along propagation, supplemented with wave model data.

The aim of this study is to track swells and observe swell attenuation across oceans using altimeter data with the help of model output, and to make a quantitative analysis of swell attenuation and nonbreaking dissipation using 10 years of global altimeter measurements. The data and the method involved in analyzing swell field are introduced in section 2. The results of swell tracking and the estimates of swell dissipation

rates are given in section 3. The results are discussed in section 4, followed by some concluding remarks in section 5.

2. Data and Methods

2.1. Data Sets

The altimeter data used in this study are from a merged and calibrated altimeter wave height database processed by the French ERS Processing and Archiving Facility (CERSAT). This data set merges the observations from a series of altimeter missions including ERS-1/2, ENVISAT, TOPEX/Poseidon, Jason-1/2, GEOSAT Follow-on and Cryosat-2 and is carefully validated against buoy measurements and jointly calibrated by cross altimeter comparisons. It can be regarded as a homogeneous and consistent data set of altimeter SWH measurements. More detailed information about this database can be found at URL http://tinyurl.com/kg7kofg.

The model output of wave parameters used here is spectra computed by WW3 versions 4.11 with physical parameterizations of *Ardhuin et al*. [2010]. The accuracy of wave parameters of the model output has been verified against measurements from buoy measurements, showing a good agreement [*Delpey et al*., 2010]. The direction and wave period errors of wave partitions in WW3 is generally less than 10° and 1 s [*Stopa et al*., 2015], which is comparable with the errors of SAR [*Collard et al*., 2009]. The WW3 output used here is on a 0.5° by 0.5° grid covering the entire ocean with the temporal resolution of 3h. The output spectrum is discretized in 32 exponentially spaced frequencies from 0.038 to 0.72 Hz, and in a 15° directional resolution with 24 directions. Output spectra are partitioned using the method of *Hanson and Phillips* [2001]. The 10 m wind speed data from the National Centers for Environmental Prediction (NCEP) Climate Forecast System Reanalysis (CFSR), which drive the model, are also employed here as an auxiliary data set. The model output fields and their detailed information are available at URL http://tinyurl.com/yetsofy.

Nearly 10 years of data of altimeter observation and model output from the period January 2003 to March 2012 are selected in the present study to track the source of swells. The wave parameters of WW3 output are interpolated into the spatiotemporal positions of altimeter measurements. Using this way, every record of altimeter-observed SWH can be collocated with a set of wave parameters from the WW3 output. Because altimeter cannot separate wind-sea and swell or distinguish different swell components, its measurements can be selected as representative measurements of swell height only when all of the following criteria are met:

1. The SWH measured by the altimeter is larger than 0.7 m and less than 5.0 m. The error model of SWH measured by the altimeter can be expressed as:

$$\sigma_{ALT}=0.10+0.05H_{s,a} \tag{1}$$

where $H_{s,a}$ is the SWH measured by the altimeter. This error model is fitted from the standard deviation (STD) curve in *Queffeulou et al*. [2011]. Given this model, the relative error of SWH is:

$$\delta_{ALT}=\sigma_{ALT}/H_{s,a}=0.10/H_{s,a}+0.05 \tag{2}$$

Therefore, the relative error of SWH increases with the decrease of SWH. Here we only select the cases of SWH larger than 0.7 m to guarantee that the relative error of SWH, δ_{ALT}, is less than 20%. Because the records employed to measure nonbreaking swell dissipation in this study are all more than 4000 km from the source point and the SWH is rarely more than 5.0 m after the propagation of 4000 km, the records with SWH of larger than 5.0 m are discarded. This is also to guarantee that the steepness of the employed swell events is small in order to reduce the probability of wave breaking.

2. The difference between the total SWH and the SWH of the most energetic partition from the WW3 output is less than the error of altimeter SWH measurements:

$$H_{s,m}-H_{ss,m}<\sigma_{ALT} \tag{3}$$

where $H_{s,m}$ is the total SWH from the WW3 output, $H_{ss,m}$ is the SWH of the most energetic partition, and σ_{ALT} is the error of altimeter-measured SWH. Under this circumstance, the most energetic partition overwhelms the other partitions so that the SWH measured by the altimeter can be approximated to the SWH of the most energetic partition. When the most energetic partition is a swell, the altimeter-measured SWH can be regarded as the measurement of swell SWH.

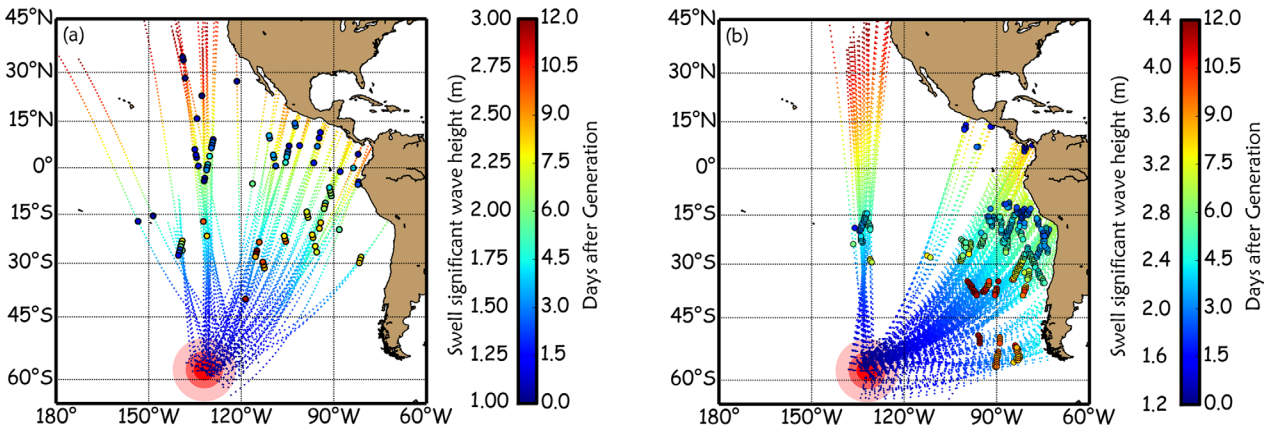

Figure 1. Back tracking the swell observations using (a) SAR wave mode data, and verifying the storm with (b) collocated alitmeter-WW3 data. The associated storm of 15 May 2011 is marked by the red disk centered in 58°S, 132°W. The colors of the swell trajectories represent the number of days since 15 May 2011. The dots with rim indicate the observation locations and their inner colors indicate the observed swell SWH. It is noted that the data of swell SWH and days after generation share the same color bar but using different maps.

3. The difference between the WW3 total SWH and the altimeter SWH is less than twice the altimeter SWH error:

$$|H_{s,a} - H_{s,m}| < 2\sigma_{ALT} \tag{4}$$

This is simply a quality control to the data set, which makes sure that the model SWH and altimeter SWH are consistent. If this difference is too large, the model output is regarded as being not reliable so that the record cannot be employed in this study.

4. The peak period of the most energetic partition from the WW3 is larger than 11.5 s, and the wave age, c_p/U, of that partition is larger than 1.6, where c_p is the phase speed calculated from the wave period and U is the 10 m wind speed from CFSR. This last criterion is to make sure that the dominant partition with the most energy is, in fact, a swell. Here the wave period threshold of 11.5s and the wave age threshold of 1.6 are relatively strict criteria, although *Kinsman* [1965] recommends the wave period threshold of 10 s and *Pierson and Moskowitz* [1964] recommend the wave age threshold of 1.2.

The Level 2 (L2) wave spectra retrieved by the quasi-linear algorithm [*Chapron et al.*, 2001] from ENVISAT are also employed to locate the position of swell sources. Original L2 SAR data are provided by the European Space Agency (ESA) and are analyzed and qualified using the swell tracking and source searching methodology developed by Collecte Localisation Satellites (CLS), which is detailed in *Husson* [2012]. The method of tracking swell using SAR data is generally the same with that of *Collard et al.* [2009] and *Ardhuin et al.* [2009], but it is more systematic by providing additional methods to find and track swells. This data set provides not only the spatiotemporal location of the center of the swell sources but also the diameters and durations of the center storms.

2.2. Swell Tracking

After collocating altimeter data and model output, each record has the necessary information of swell SWH, peak wave period, and peak wave direction, required to estimate the dissipation rate. Based on these data, the analysis of swells can be conducted using a method similar to *Ardhuin et al.* [2009]. Following their methodology, the first step is to identify swell sources. This step has been done in the analysis SAR data set provided by CLS. Using the algorithm developed by *Husson* [2012], the approximated diameter and duration of each storm can be estimated from the size of the convergence area. Only the storms with the diameters $d \leq 1600$ km and durations $\tau \leq 36$ h are retained, and the identified swell sources are also verified by back propagating the collocating altimeter-WW3 data set. This extra step helps remove wrong-identified sources introduced from the direction and period errors. An illustration of tracking swell to identify the swell source of 15 May 2011 centered in 58°S, 132°W is shown in Figure 1, with the result of SAR wave mode tracking in Figure 1a, and the result of verification using the collocation data set in Figure 1b.

In the next step, the records in the collocation data set are associated with different swell sources, that is, to find the corresponding storm of each measurement. Given the time and locations of both the swell source

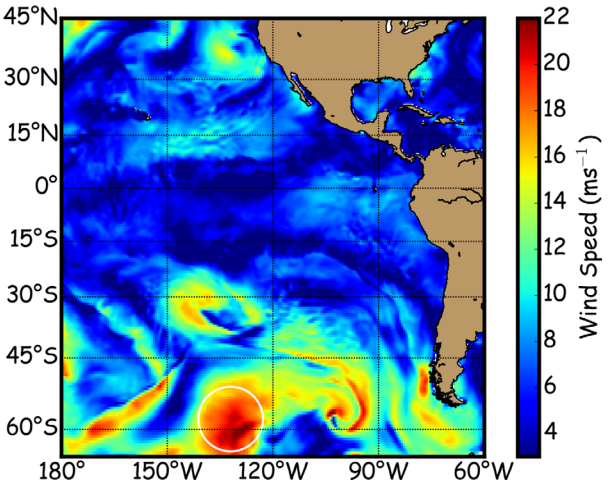

Figure 2. The distribution of wind speed from CFSR on 15 May 2011. The region with a white circle corresponds to the swell source of 15 May 2011 centered in 58°S, 132°W which is identified by back tracking SAR data.

and the altimeter measurement, the peak period and direction needed to propagate between them are calculated using the linear propagation model of swell presented by *Barber and Ursell* [1948]. If the wavelength and direction in the record are found within ±50 m and ±10° of their expected values, the record is associated with the source.

To demonstrate the effectiveness of this simple scheme, an example of organizing a swell field using model output information is presented. Figure 2 shows the distribution of wind speed from CFSR on 15 May 2011. It is clear from the figure that a well-defined storm region with the highest wind speed more than 20 m s^{-1} can be observed at approximately 60°S, 130°W, validating the swell source information from the SAR data set. Although there is a slight deviation between the geometrical centers of the storm defined by the wind and of the swell source, it is noted that the storm "center" itself is an ambiguous definition and varies under different circumstances. Figure 3 represents the wave partition associated with this swell source in the WW3 output, with results given at 2 days intervals from 19 May 2011. The criteria of associating wave partition and swell source provide a coherent swell field among many wind-sea and swell components, and this coherence remains even when the swell field is far from the source. The structure of this swell field is similar to that presented by *Delpey et al.* [2010], with the "stretch" of the swell field and the attenuation of

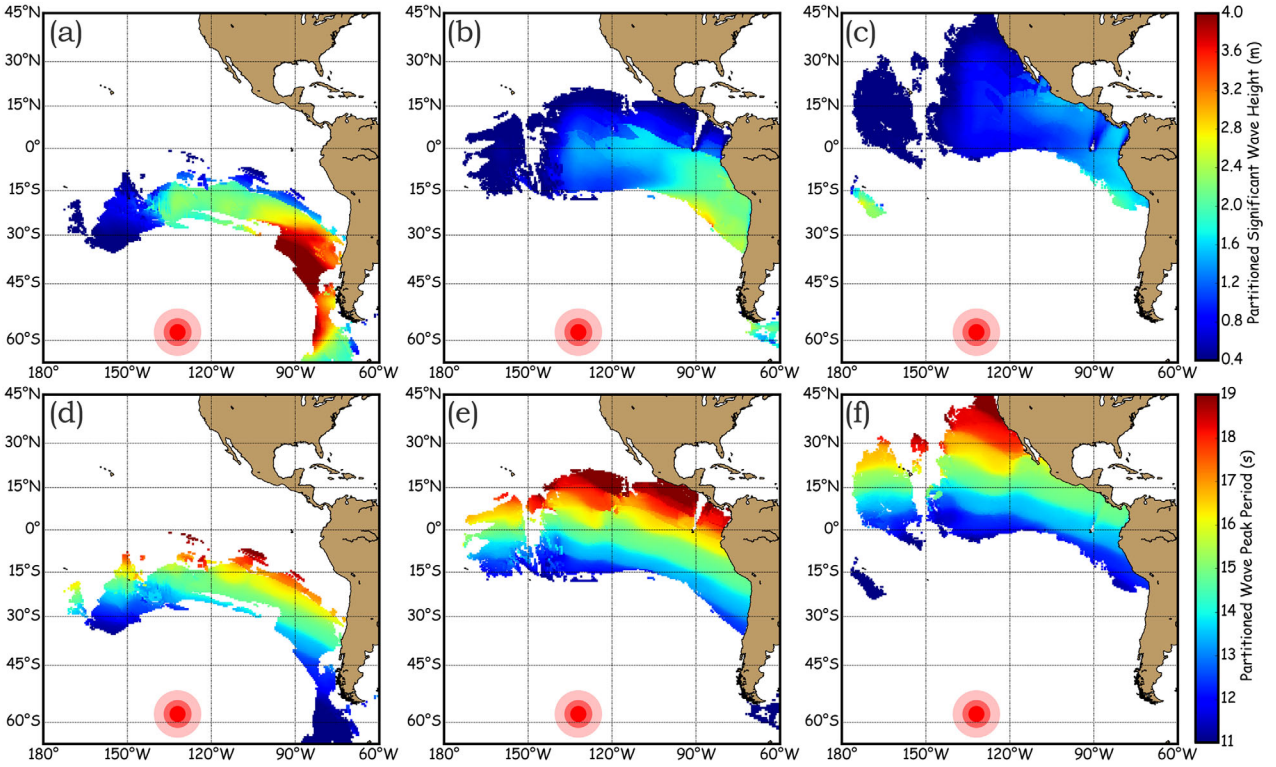

Figure 3. The swell height (top) and peak period (bottom) of the swell field associated with the swell source of 15 May 2011 centered in 58°S, 132°W (the red disk). The wave parameters and partition information are from the WW3 output. The swell system is illustrated on (a and d) 19 May, (b and e) 21 May, and (c and f) 23 May.

wave height mainly induced by frequency dispersion and angular spreading effect being clearly visible. This result shows that this swell tracking procedure can effectively filter the swells from other systems. Therefore, most of the remained records in the collocated data set can be attributed to a swell source.

The records within 4000 km of the source are ignored to only remain the data of "far field" measurements to guarantee the validity of the point source assumption [*Collard et al*., 2009]. If the group speed of swells is strongly affected by the surface current or other refraction effects, the measurement of the swell will not be associated with its source. Therefore, this step also excludes the impact of strong surface currents and other factors causing the change of swell group speed. The record is discarded if waters shallower than 300 m are within 10 km of the swell track so that little energy can be blocked during propagation. The record with the propagation track passing high wind speed regions ($c_P/U < 1.6$) is also discarded to minimize the impact of local wind/wind-sea and the effect of nonlinear wave-wave interaction. The remained records are merged into initial direction and wavelength bands (here, 5° wide for direction and 50 m wide for wavelength) to increase the amount of observations for each swell track. Only the swell tracks with observations spanning more than 3000 km along the great circle and with more than 4 altimeter tracks intersected are retained. These criteria are made to be strict to ensure the quality of measurements as well as the robustness of the estimation of swell attenuation and dissipation rates. After applying all these selection criteria, the final database consists of 202 swell events with wavelengths ranging from 250 to 500 m, which could extend the data amount of related field experiments.

2.3. Attenuation and Dissipation Estimation

As mentioned before, the attenuation of swell is constituted of many processes which cannot be easily separated. If all the processes are combined together, it is hard to find a unified formula of how the swell attenuate with the distance from the source. Therefore, we simply assume that the attenuation of swell energy follows the exponential relation:

$$E_s(\alpha_i) = E_s(\alpha_0)\exp\left[-R\mu_a(\alpha_i-\alpha_0)\right] \tag{5}$$

where E_s is the swell energy, R is the Earth radius, α is the angular distance from the source point, α_0 is the reference angular distance corresponding to 4000 km, α_i is the angular distance from the source of measurements, and μ_a is the attenuation rate. One value of μ_a is estimated for each swell track using least square fitting after applying a logarithm transformation to the equation, and the data from all the tracks are also merged into one group to give a robust estimation of μ_a.

Although the attenuation rate can give an overall view on how swell evolve when propagation, it cannot show the impact of different effects. In fact, frequency dispersion, angular spreading and dissipation are often regarded as the three most important processes in swell attenuation [*Collard et al*., 2009]. *Collard et al*. [2009] also demonstrate that E_s decreases as asymptotically as $1/[\alpha\sin(\alpha)]$ without dissipation. The factor α relates to the dispersion and the $\sin(\alpha)$ factor is due to the angular spreading on the spherical surface. They also demonstrate that the error of asymptotic E_s is less than 20% when swells propagate more than 4000 km away from the storm center in the absence of dissipation. Therefore, they select the distance of 4000 km as a criterion of "far field," and this criterion is also used in *Ardhuin et al*. [2009]. The bound of far field here is also set as 4000 km, and records within 4000 km from the source are discarded. Because swells have long wavelength and the wave heights are moderate after propagating 4000 km from the source, wave breaking should be rare and the rate estimated here can be regarded as the nonbreaking dissipation rate.

For each swell track, if the spatial dissipation rate μ is constant, the E_s will only be a function of α. The spatial evolution rate defined by *Ardhuin et al*. [2009] is used:

$$\mu = -\frac{\mathrm{d}(E_s\alpha\sin\alpha)/\mathrm{d}\alpha}{RE_s\alpha\sin\alpha} \tag{6}$$

The method of estimating μ here is also similar to that of *Ardhuin et al*. [2009], and uses the following equation of linear dissipation model to determine the values of μ and E_s (α_0):

$$E_s(\alpha_i)\alpha_i\sin\alpha_i = E_s(\alpha_0)\alpha_0\sin\alpha_0\exp\left[-R\mu_a(\alpha_i-\alpha_0)\right] \tag{7}$$

The best-fitted pair of $[E_s(\alpha_0),\mu]$ is estimated for each swell track using least square method after applying a logarithm transformation to the equation.

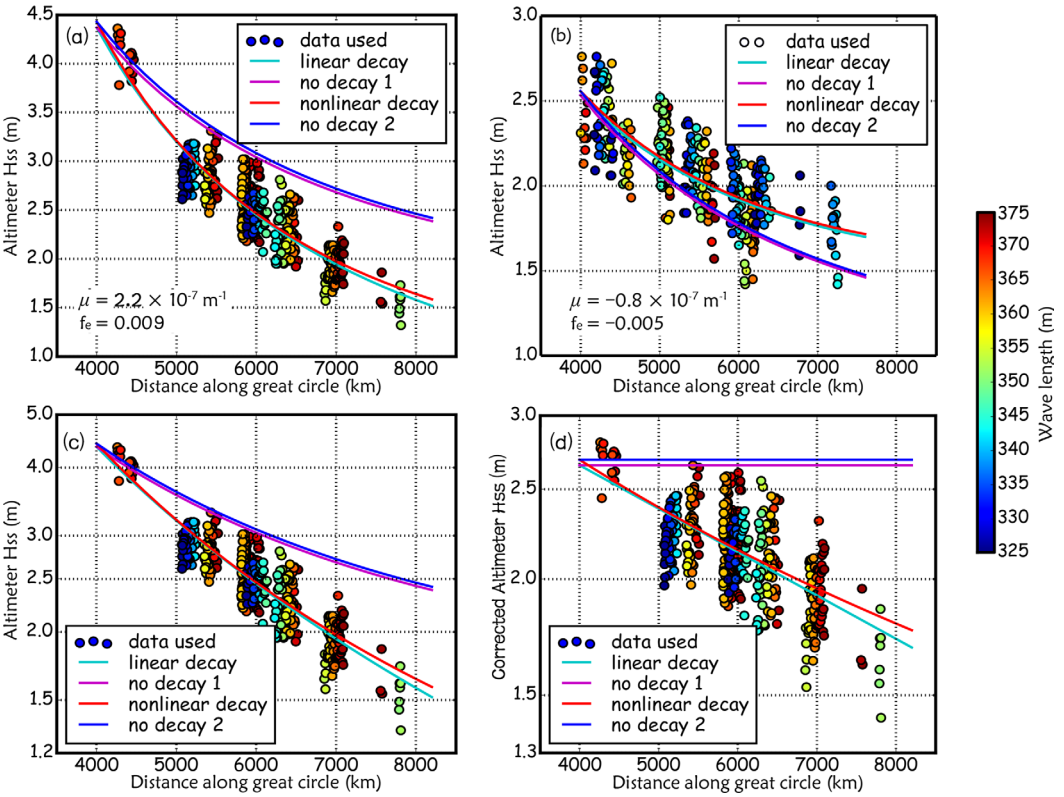

Figure 4. Observed swell SWH as a function of distance from the storm center, overlaid with theoretical decays with fitted dissipation rate using linear dissipation model (cyan line) and nonlinear dissipation model (red line). The curves of no dissipation with the same 4000 km wave height as linear dissipation condition (magenta line) and nonlinear dissipation condition (blue line) are also shown as a reference. The color of the dot indicates the wavelength of each measurement. (a and b) Two swell packets with a positive and a negative values of estimated spatial evolution rate generated respectively by the storm on 20 November 2007, centered at 44°N, 168°E, and the storm on 10 July 2011, centered at 48°S, 42°W. (c) Same as Figure 4a but is shown in semi-log coordinates for reference. (d) Same as Figure 4b, but the wave height, $H_{ss}\sqrt{\alpha \sin \alpha}$, is corrected by removing the effect of dispersion and angular spread and is also shown in semi-log coordinates.

Although widely used in the literature, the above linear dissipation model has little basis in wave physics. Therefore, the dissipation rates are also estimated using a nonlinear decay model derived from a mechanism of wave coupling with turbulent atmospheric boundary layer, which is also given by *Ardhuin et al.* [2009]:

$$\beta = -\frac{dE_s/dt}{E_s} = C_g\mu = 64\frac{\rho_a\pi^2}{\rho_w g T^2} f_e u_{orb} \tag{8}$$

where orbital velocity u_{orb} is given by $u_{orb}=4\pi\sqrt{E_s}/T$, and the density of water and air, ρ_w and ρ_a, are approximated to 1.03×10^3 kg m^{-3} and 1.3 kg m^{-3}, and the f_e is the nonlinear swell dissipation factor to be fitted. The formulation of this mechanism is equivalent with the mechanism of turbulent flow on the water side of the air-sea interface, which is proposed by *Babanin* [2012]:

$$\frac{da^2(x)}{dx} = -\frac{4}{3} b_1 k^2 a^3 \tag{9}$$

where a and k are the amplitude and the wave number of swell, and b_1 is the corresponding dissipation factor. A constant f_e and b_1 is then fitted for each swell track. Some other potential mechanisms and formulas of swell dissipation are also presented [e.g., *Donelan et al.*, 2012]. However, in this study, only one linear and one nonlinear model was employed and these three parameters, μ, f_e and b_1, are calculated as references.

3. Results

Two typical examples of swell tracks are illustrated in Figure 4 with the observed swell wave height against the distance from the swell source. The evolution of swell height along the great circle can be clearly

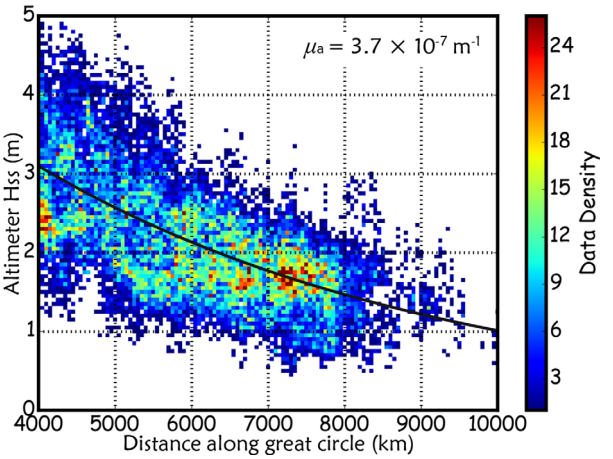

Figure 5. Observed swell SWH as a function of the distance from the storm center for all recorded altimeter measurements of the 202 cases, overlaid with the best fitting curve represented by equation (5). The color scale depicts data density within a 50 km ×0.05 m grid box. The data set contains more than 28,000 data points.

observed, showing that the SWH decreases along the propagation. A more general result of swell SWH against the distance along the great circle is shown in Figure 5, which contains all the 28,167 data points from 202 swell tracks. A best fitting curve of equation (5) is overlaid on the plot with a μ_a of $(3.7 \pm 0.2) \times 10^{-7}$ m^{-1} (at 99.9% significance level). It is not surprising that there is scatter from the curve in the plot because different swells have different initial SWH. The value of μ_a of each swell track is also estimated and the mean value of all μ_a stays 3.7×10^{-7} m^{-1}, showing the robustness of the estimation. As can be seen in Figure 5, the exponential relationship can approximate the shape of the attenuation curve quite well, although there is no physics underpinning it.

After the data being corrected using the $1/[\alpha \sin(\alpha)]$ relation derived from the source point model [*Collard et al*. 2009], as shown in Figure 4d, the nonbreaking dissipation rate μ is estimated for each swell track. The estimated μ ranges from -1.9 to 4.6×10^{-7} m^{-1}, with a mean and a median of both 0.8×10^{-7} m^{-1} and an STD of 1.2×10^{-7} m^{-1}. This result is comparable to -0.6 to 3.7×10^{-7} m^{-1} reported by *Ardhuin et al*. [2009] and 0 to 2×10^{-7} m^{-1} reported by *Snodgrass et al*. [1966], while significantly lower than the value of 14×10^{-7} m^{-1} reported by *Young et al*. [2013] (In *Young et al*. [2013], their μ is estimated based on the exponential evolution of SWH but not wave energy, and a factor of 2 is multiplied to their 7×10^{-7} m^{-1}.). The different fitted curves overlaid in Figure 4 denote different models of theoretical decay (and no decay). The μ value in Figure 4a is positive, which corresponds to energy loss in propagation, while the μ value is negative in Figure 4b, which corresponds to energy growth. However, it should be noted that the SWH is always decreasing along propagation even when μ is negative, showing the importance of frequency dispersion and angular spreading effects.

A dependence between swell dissipation rate μ and wave steepness at 4000 km is illustrated in *Ardhuin et al*. [2009]. The relationship between μ and wave steepness at 4000 km from the swell source estimated from the altimeter measurements is shown here in Figure 6a. The correlation coefficient between μ and $H_{ss,4000}/L$ is 0.49, which is at the 99.9% significance level (The threshold of 99.9% significance level is 0.26 for a freedom of 200). The dependences of the dissipation rates on wavelength, wind speed, and wave age are

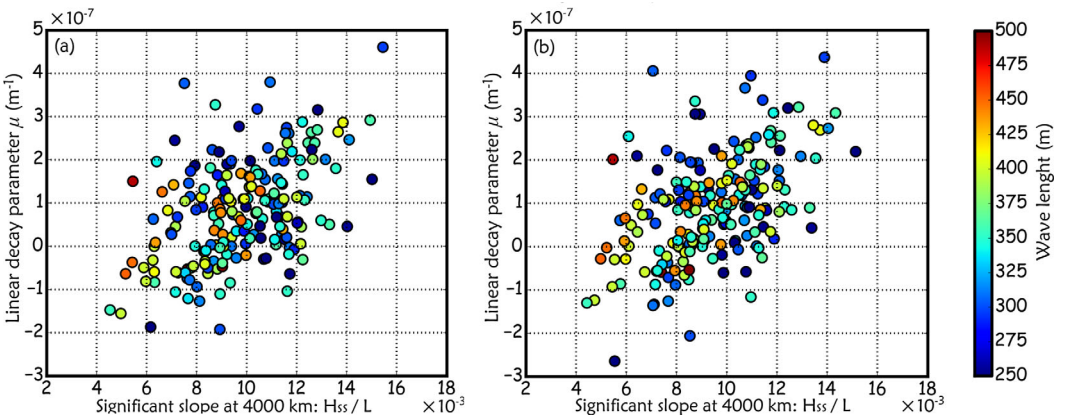

Figure 6. Linear decay parameter as a function of the wave steepness at 4000 km, for different wavelengths (colors) based on 202 events fitted by (a) direct altimeter-measured SWH, and (b) altimeter-measured SWH corrected with the energy proportion of the most energetic swell system in WW3.

also tested, but the correlation coefficients are all not more than 0.3. Therefore, the result here also shows that there is a significant dependence between dissipation rate and wave slope, although this dependence is not simply linear.

Some error terms are introduced during the estimation and need to be considered. Because the total SWH is used to approximate swell SWH, the altimeter-measured SWH is also corrected with the energy proportion of the most energetic swell in the WW3 output. The results after the correction are shown in Figure 6b. After correction, the estimated μ changes very little and ranges from -2.6 to 4.4×10^{-7} m^{-1}, and the correlation coefficient between the dissipation rate and wave steepness is 0.51, which is almost unchanged. For different swell cases, the mean value of the differences between μ before and after this correction is less than 0.1×10^{-7} m^{-1}, and the STD of the difference is 0.3×10^{-7} m^{-1}. This demonstrates the statistical significance of the result and altimeter-measured SWH being a reasonable approximation of the swell height. It also shows that this approximation can introduce an error in μ of about 0.3×10^{-7} m^{-1}. Also, the errors in altimeter-measured SWH can introduce an average error in μ of about 0.1×10^{-7} m^{-1}, estimated by the error model given by equation (1) and the same perturbation method as presented in *Ardhuin et al*. [2009]. During the least square fitting, minimization of the mean square differences of different parameters are tested, including $E_s(\alpha_i)$, $E_s(\alpha_i)\alpha_i \sin\alpha_i$, and $\log[E_s(\alpha_i)\alpha_i \sin\alpha_i]$. It was found that minimization of different parameters can also introduce an error in μ of about 0.2×10^{-7} m^{-1}. Besides these errors, the deviation of E_s relative to the asymptote due to the storm shape can produce an error in μ of 0.5×10^{-7} m^{-1} [*Ardhuin et al*., 2009]. Taking all these terms into account, the total errors are comparable to the measured nonbreaking dissipation rates. Therefore, although 49 negative values of μ are found, most of them are not statistically significant considering these errors.

For the fitted result of nonlinear dissipation, the estimated f_e ranges from -0.013 to 0.027, with a median of 0.004, which is also comparable with the results of *Ardhuin et al*. [2009] (-0.004 to 0.019). Because of the same formulation, this range can be related to the dissipation rate b_1 presented in *Babanin* [2012] using the equation in *Young et al*. [2013]:

$$b_1 = 24 f_e \rho_a / \rho_w \tag{10}$$

According to this equation, $b_1 \approx f_e/33$ in the swell tracks presented here, and thus b_1 ranges from -0.0004 to 0.0008.

Magnifying all possible the error terms, a relaxed bound of the dissipation parameters, -2.5×10^{-7} m^{-1} $< \mu < 5 \times 10^{-7}$ m^{-1}, or $-0.015 < f_e < 0.03$, or $-0.0005 < b_1 < 0.0009$, can be obtained (respectively under the precision of μ: 0.5×10^{-7} m^{-1}, f_e: 0.005, and b_1:0.0001). These bounds are wide enough so that it can be employed as an acceptance range to test the validity of model parameterization and other field experiment results. For example, the results of *Snodgrass et al*. [1966] and *Ardhuin et al*. [2009] are within this bound, while those of *Young et al*. [2013] are not. Although altimeters are used both in the present study and *Young et al*. [2013], the mean value of the dissipation rate in this study is an order of magnitude smaller than that of *Young et al*. [2013], indicating there should be some problem in their methodology. The reason for this difference is discussed in section 4.

4. Discussion

Both the present study and *Young et al*. [2013] select the wave height measurements from altimeters. However, the dissipation rate of *Young et al*. [2013] falls out of the acceptance range of dissipation rate derived by this study. In fact, their result is even larger than the largest attenuation rate μ_a in all the swell events in this study (the maximum of attenuation rate here is 9.5×10^{-7} m^{-1}).

The main difference between these two studies is the ways of dealing with the effects of frequency dispersion and angular spreading. Here the data are selected in the far field and corrected by the $1/\alpha \sin(\alpha)$ point source model given by *Collard et al*. [2009]. Although this model slightly simplifies the situation of the real ocean, it is demonstrated to work well for the swell in the far field, and the error of the dissipation rate introduced by this approximation can be also estimated [*Ardhuin et al*., 2009]. The acceptance range of dissipation rate derived by this way is reasonable. However, the data used in *Young et al*. [2013] are in the near field so a point source model is not applicable. *Young et al*. [2013] assume that the swells come from a quasi-stable storm and the sampling is made in a near field so that the SWH in a certain location can be

regarded as a constant over propagation time and frequency dispersion will not influence the swell height. Their swell tracking method is reasonable if this assumption is valid. However, in their Figure 4, monotonic SWH variations of 0.5–1.5 m can be found in a 36 h time window sometimes (This time window corresponds to the time for 13s swells to propagate 1400 km), which, to our understanding, suggests that the wave heights are not constant over propagation time. Under their assumption, the wave periods of the wave in one altimeter transect should also be in a narrow band. To test the rationality of this assumption, we apply the same method and the same data selection criteria as *Young et al*. [2013], and the selected altimeter transects are collocated with model output to obtain the wave period along transects. The result shows that the dispersion is obvious with peak wave period sometimes varying more than 2 s monotonically in 1400 km along their altimeter transects (the results are not shown here). Furthermore, there can be more than two main swell systems present along the altimeter track in some cases, adding to the uncertainties in estimating the dissipation rate of their scheme. Therefore, it seems that using altimeter data from instantaneous transects is not a feasible method to measure the swell dissipation, as dispersion effect cannot be ignored.

The angular spreading is also ignored in the analysis of *Young et al*. [2013] because the shape of the swell source is unknown. For a monochromatic swell from one point source without dispersion, only the angular spreading effect needs to be taken into account. The attenuation rate caused by angular spreading for a point source model will increase with the decrease of the distance from the source when the angular distance from the source is less than $\pi/2$, because the angular spreading follows the relation of $1/\sin\alpha$ (of which the derivative is $-\cos\alpha/\sin^2\alpha$, monotonically increasing from negative infinite to zero in $(0, \pi/2]$). However, a point source is not valid in the near field as the size of the storm is comparable to the propagation distance. For a near field condition, the angular spreading is illustrated in Figure 7. The swell source at shade area propagate the energy to the observation points C and D. The observation point C can receive the energy in an angular range of θ_1, while D can receive the energy in that of θ_2, so that the wave energy of C at a given frequency will be larger than that of D. This intuitionistic illustration can well represent the principle of angular spread. It is not difficult to prove that the derivative of the angular range θ also monotonically increases with the distance. This analysis is based on a uniform spectra in the source region, and the real wave field is a lot more complex than that. However, it is applicable to qualitatively explain a basic law of swell propagation: the shorter the distance is from the swell source, the stronger the effect of angular spread on the wave energy will be, and vice versa, despite the shape of the storm and the model of the swell source. This law can also be easily demonstrated using an ideal model experiment. The cases in *Young et al*. [2013] are all in the near field so that the angular spreading dominates swell decay. Therefore, their resulting dissipation rate also contains the attenuation due to angular spreading effect.

Although based on different physical mechanisms (in fact, no strict physical underpins μ), both linear and nonlinear decay relations fit the results well for most swell tracks. The accuracy of the observations is still not enough to determine the formula and mechanism of swell dissipation only from swell SWH observations of each swell track. Therefore, other potential formulas of swell dissipation are not fitted here. The vague but statistically significant dependence of dissipation rate on wave steepness implies that the mechanisms of turbulence interactions proposed by *Ardhuin et al*. [2009] and *Babanin* [2012] are still possible, and there is also possibility that these two mechanisms coexist. However, the correlation coefficient derived here is not large enough to be hired as the evidence. In fact, the correlation coefficient of about 0.85 in *Ardhuin et al*. [2009] is not more significant than the result here given the critical value of 99.9% significance level is 0.65 for $N=22$. Therefore, the small but statistically significant correlation coefficient indicates that there may be other parameters and processes having impacts on the nonbreaking dissipation besides turbulence interactions in the air and water.

Some negative but not significant values of dissipation rate μ are found in *Ardhuin et al*. [2009], and these negative values also widely exist in the present result. If these negative values are authentic and not due to measurements errors, the mechanism of turbulence interactions cannot explain these points despite the significant correlation. To check these negative values, the statistical distribution of the values of dissipation rate is shown here in Figure 8, which shows a similar distribution to a normal one with the same mean and STD. From this distribution, it is found that, on the one hand, no clear boundary can be observed between positive and negative values. One the other hand, the STD of the distribution is close to the superstition of errors analyzed in section 3, which suggests that the scatter and the negative values of the dissipation rates

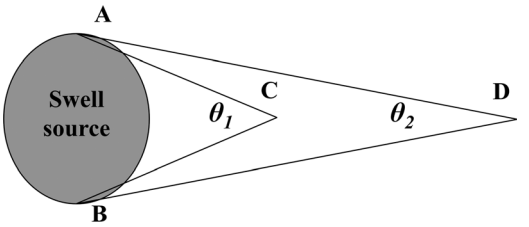

Figure 7. Illustration of swell angular spreading effect. The swell source (shade area) propagate the energy to the observation points C and D.

might be caused by these errors. It can be understood that a negative value of dissipation rate might be obtained for a "positive dissipation" process considering these errors. Given these negative values are not statistically significant, it is a reasonable conjecture that these negative values are due to the measurement errors. However, numerous studies have also shown some evidence that a strong coupling of swell with atmospheric boundary layer and shorter wind waves may lead to the swell amplification [e.g., *Benilov et al*., 1974; *Badulin and Grigorieva1*, 2012]. Therefore, it will be still helpful to inspect the ocean environment, especially the wind and short wind-sea situation, along the swell tracks. The wind speed and wind-sea (waves with peak periods less than 8 s and wave ages less than 1) SWH are checked along the propagation track of each wave packet. No regular pattern is found and the difference of wind speed and short wave height along swell tracks between negative values ($\mu < -1.0 \times 10^{-7}$ m^{-1}) and maximal positive values ($\mu > 2.5 \times 10^{-7}$ m^{-1}) of dissipation rates is hardly distinguishable. Therefore, the negative values in this study cannot be hired as observational evidence directly to support the points of view of swell amplification. This does not mean that the swell amplification, as well as its mechanism, does not exist in the swell evolution. It is also possible that the negative values of the spatial evolution rates are the result of both errors and swell amplification effect, while the swell amplification is overwhelmed by the errors. However, more advanced tools and methods, as well as more data, are needed to have a better understanding of this issue.

However, no matter what mechanisms or physical processes are involved, the dissipation rate itself is an important parameter as demonstrated in theoretical studies and numerical models [e.g., *Hanley and Belcher*, 2008; *Ardhuin et al*., 2010]. For example, this acceptance range can be employed as a reference for "tuning" swell dissipation in wave model experiments. In fact, because the nonbreaking dissipation is generally small, corresponding to an e-folding scale of more than 2000 km, it is practicable to regard it as a constant in some applications. Since the distribution of dissipation rates is normal-like and the STD is close to the superstition of errors, a statistical average of the observational dissipation rates can be used as a recommended value in practice, according to the central limit theorem. Based on the altimeter observation, we recommend the nonbreaking swell dissipation rate of $\mu \approx 1 \times 10^{-7}$ m^{-1}, $f_e \approx 0.004$ and $b_1 \approx 0.0001$ (one significant digit for all coefficients) for the parameterization in wave modeling. These values are close to the values applied in *Ardhuin et al*. [2010] and *Zieger et al*. [2015], again showing the validity of the results.

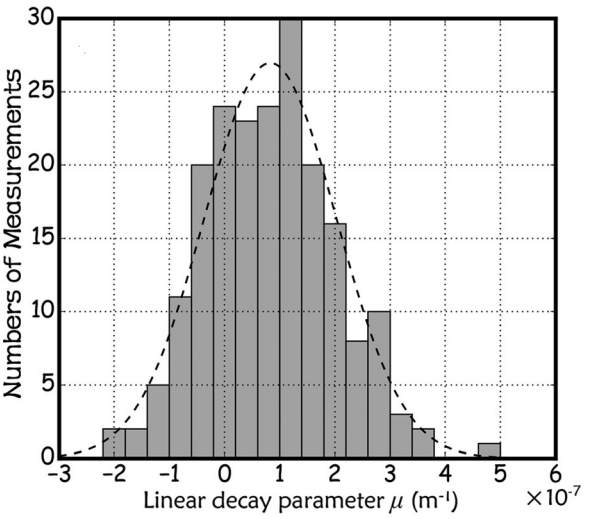

Figure 8. The statistical distribution for the nonbreaking dissipation rates derived from altimeter data. The overlaid dash line is the corresponding normal distribution for reference with a mean of 0.8×10^{-7} m^{-1} and an STD of 1.2×10^{-7} m^{-1}.

Considering the value of dissipation rate, the present study did not achieve a more narrow range than *Ardhuin et al*. [2009]. However, because of the larger amount of swell cases used, more measurements for each event, and better accuracy of altimeter SWH, the confidence level of this range were significantly improved and the range in this study can be regarded as an acceptance range for future studies. A noteworthy feature is that the sum of all error terms is already comparable to the order of magnitude of the swell dissipation rate itself in both this study and *Ardhuin et al*. [2009]. Among all error terms, the largest one comes from the assumption of swell point source which contributes about 0.5×10^{-7} m^{-1}. Therefore, this range is probably the limit that can be achieved

from observations based on the point source model and the swell tracking scheme proposed by *Collard et al*. [2009]. To improve the accuracy of these field experiments, better swell source models or different methods of tracking swell are needed.

5. Conclusions

The attenuation and nonbreaking dissipation of swell have received attention recently. In spite of this, the quantitative knowledge on this issue is believed to be generally poor because little experimental data are available and designing field experiments to measure swell evolution is a challenging task. Taking advantage of high-quality data from space-borne altimeters and wave model output, ocean swell trains propagated far away from their source regions are systematically tracked across oceanic basins in the present study. After applying strict selection criteria on nearly 10 year altimeter-WW3 collocation data over January 2003 to March 2012, 202 swell events with wavelengths ranging from 250 to 500 m are captured to estimate the attenuation and nonbreaking dissipation rate of ocean swells, which effectively extends the data amount of field experiments. The present study also shows that the altimeter is a potential tool to analysis swell, especially with the assistance of wave model.

The observed attenuation and nonbreaking dissipation rate of swells are in line with previous studies using in situ data and SAR wave mode. The averaged linear attenuation rate of swells is about 4×10^{-7} m^{-1} while the averaged linear dissipation rate is about 1×10^{-7} m^{-1}. The difference between attenuation and dissipation rates shows that frequency dispersion and angular spreading are two most important processes impacting on the attenuation of swell in the far field, while the nonbreaking dissipation is secondary. By analyzing the errors of measurements, relaxed acceptance bounds of the swell dissipation rates, -2.5×10^{-7} m^{-1} $< \mu < 5 \times 10^{-7}$ m^{-1}, $-0.015 < f_e < 0.03$, and $-0.0005 < b_1 < 0.0009$, denoted by different coefficients, are also obtained. The dependence of dissipation rate on wave steepness are verified, but this dependence is not simply linear according to both the results of *Ardhuin et al*. [2009] and this study. On one hand, this indicates that the turbulence interaction is a possible process impacting swell dissipation. On the other hand, it shows there may be other physical processes playing roles in the nonbreaking dissipation of ocean swells. The result shows that the nonbreaking e-folding scales of small-amplitude swells can be as long as infinite while those of steepest swells in the far field are also at least 2000–2500 km. Some negative values of dissipation rates were observed, but it is unclear whether these points are purely due to errors or have some physical importance. More advanced tools and methods and more related data are needed for further study.

The dissipation rate of the present study can be applied to wave prediction and employed as references to other studies of swell dissipation or air-sea and wind-wave-turbulence interactions. Future research can be conducted with the accumulation of more data, to enlarge the data amount of field experiments and improve the significance of the results. The Sentinel-1A, and future Sentinel-1B, Jason-3, Sentinel-3, and CFOSAT are all potential good-quality data source for this aim. Meanwhile, improving the swell source model and developing other schemes of measuring the energy of the swell system are also promising for improving the accuracy of field experiments. Such efforts on the observation of swell dissipation are helpful for a better parameterization in numerical wave modeling and a better understanding in air-sea interactions.

Acknowledgments
The altimeter data are downloaded from the database of CERSAT, available at http://tinyurl.com/kg7kofg. The model output used for the analysis is part of the IOWAGA database, available at http://www.tinyurl.com/yetsofy. Original L2 SAR data were provided by the European Space Agency (ESA) and they were analyzed and qualified using the swell tracking methodology developed by CLS. This work is supported by the National Natural Science Foundation of China (41331172, U1406404, and 61361136001). The anonymous reviewers are greatly appreciated for their helpful comments and suggestions on this study.

References

Ardhuin, F., and A. D. Jenkins (2006), On the interaction of surface waves and upper ocean turbulence, *J. Phys. Oceanogr.*, *36*, 551–557.
Ardhuin, F., B. Chapron, and F. Collard (2009), Observation of swell dissipation across oceans, *Geophys. Res. Lett.*, *36*, L06607, doi:10.1029/2008GL037030.
Ardhuin, F., et al. (2010), Semi-empirical dissipation source functions for wind-wave models: Part I, Definition, calibration and validation, *J. Phys. Oceanogr.*, *40*, 1917–1941.
Babanin, A. V. (2006), On a wave-induced turbulence and a wave-mixed upper ocean layer, *Geophys. Res. Lett.*, *33*, L20605, doi:10.1029/2006GL027308.
Babanin, A. V. (2012), Swell attenuation due to wave-induced turbulence, paper presented at 31st International Conference On Ocean, Offshore and Arctic Engineering Division, Riode Janeiro, Brazil, 1–6 July.
Babanin, A. V., and B. K. Haus (2009), On the existence of water turbulence induced by non-breaking surface waves, *J. Phys. Oceanogr.*, *39*, 2675–2679.
Badulin, S. I. (2014), A physical model of sea wave period from altimeter data, *J. Geophys. Res. Oceans*, *119*, 856–869, doi:10.1002/2013JC009336.

Badulin, S. I., and V. G. Grigorieva1 (2012), On discriminating swell and wind-driven seas in Voluntary Observing Ship data, *J. Geophys. Res.*, *117*, C00J29, doi:10.1029/2012JC007937.
Barber, N. F., and F. Ursell (1948), The generation and propagation of ocean waves and swell. Part I. Wave periods and velocities, *Philos. Trans. R. Soc. London A*, *240*, 527–560.
Benilov, A. Y., O. A. Kouznetsov, and G. N. Panin (1974), On the analysis of wind wave-induced disturbances in the atmospheric turbulent surface layer, *Boundary Layer Meteorol.*, *6*, 269–285.
Chapron, B., H. Johnsen, and R. Garello (2001), Wave and wind retrieval from SAR images of the ocean, *Ann. Telecommun.*, *56*, 682–699.
Chen, G., B. Chapron, R. Ezraty, and D. Vandemark (2002), A global view of swell and wind sea climate in the ocean by satellite altimeter and scatterometer, *J. Atmos. Oceanic Technol.*, *19*, 1849–1859.
Collard, F., F. Ardhuin, and B. Chapron (2009), Monitoring and analysis of ocean swell fields from space: New methods for routine observations, *J. Geophys. Res.*, *114*, C07023, doi:10.1029/2008JC005215.
Delpey, M. T., F. Ardhuin, F. Collard, and B. Chapron (2010), Space-time structure of long ocean swell fields, *J. Geophys. Res.*, *115*, C12037, doi:10.1029/2009JC005885.
Donelan, M. A., M. Curcic, S. S. Chen, and A. K. Magnusson (2012), Modeling waves and wind stress, *J. Geophys. Res.*, *117*, C00J23, doi:10.1029/2011JC007787.
Grachev, A. A., and C. W. Fairall (2001), Upward momentum transfer in the marine boundary layer, *J. Phys. Oceanogr.*, *31*, 1698–1711.
Hanley, K. E., and S. E. Belcher (2008), Wave-driven wind jets in the marine atmospheric boundary layer, *J. Atmos. Sci.*, *65*, 2646–2660.
Hanson, J. L., and O. M. Phillips (2001), Automated analysis of ocean surface directional wave spectra, *J. Atmos. Oceanic Technol.*, *18*, 277–293.
Hasselmann, K. (1963), On the non-linear energy transfer in a gravity-wave spectrum. Part 3. Evaluation of the energy flux and swell-sea interaction for a Neuman spectrum, *J. Fluid Mech.*, *15*, 385–398.
Högström, U., A. Rutgersson, E. Sahlée, A.-S. Smedman, T. S. Hristov, W. M. Drennan, and K. K. Kahma (2013), Air–sea interaction features in the Baltic Sea and at a Pacific Trade-Wind Site: An inter-comparison study, *Boundary Layer Meteorol.*, *147*, 139–163.
Husson, R. (2012), Development and validation of a global observation-based swell model using wave mode operating Synthetic Aperture Radar, PhD thesis, Dep. of Earth Sci., Univ. of Bretagne occidentale, Brest, France. [Available at http://tinyurl.com/kzm434f.]
Jiang, H., and G. Chen (2013), A global view on the swell and wind sea climate by Jason-1 mission: A revisit, *J. Atmos. Oceanic Technol.*, *30*, 1833–1841.
Kinsman, B. (1965), *Wind Waves*, 676 pp., Prentice Hall, Englewood Cliffs, N. J.
Munk, W. H., G. R. Miller, F. E. Snodgrass, and N. F. Barber (1963), Directional recording of swell from distant storms, *Philos. Trans. R. Soc. London A*, *255*, 505–584.
Perignon, Y., F. Ardhuin, M. Cathelain, and M. Robert (2014), Swell dissipation by induced atmospheric shear stress, *J. Geophys. Res. Oceans*, *119*, 6622–6630, doi:10.1002/2014JC009896.
Pierson,W. J., and L. Moskowitz (1964), A proposed spectral form for fully developed wind seas based on the similarity theory of S. A. Kitaigorodskii, *J. Geophys. Res.*, *69*, 5181–5190.
Queffeulou, P., F. Ardhuin, and J.-M. Lefèvre (2011), Wave height measurements from altimeters: Validation status and applications, paper presented at OSTST Meeting, Ocean Surface Topography Science Team, San Diego, Calif., 19–21 Oct. [Available at http://tinyurl.com/nx49anh.]
Semedo, A., O. Saetra, A. Rutgersson, K. Kahma, and H. Pettersson (2009), Wave-induced wind in the marine boundary layer, *J. Atmos. Sci.*, *66*, 2256–2271.
Snodgrass, F. E., G. W. Groves, K. Hasselmann, G. R. Miller, W. H. Munk, and W. H. Powers (1966), Propagation of ocean swell across the Pacific, *Philos. Trans. R. Soc. London A*, *249*, 431–497.
Stopa, J. E., F. Ardhuin, A. V. Bababin, and S. Zieger (2015), Comparison and validation of physical wave parameterizations in spectral wave models, *Ocean Modell.*, doi:10.1016/j.ocemod.2015.09.003, in press.
Tolman, H. L., and The WAVEWATCH III® Development Group (2014), User manual and system documentation of WAVEWATCH III® version 4.18, *Tech. Note 316*, 282 pp., NOAA/NWS/NCEP/MMAB, U. S. Dep. of Commer., Natl. Ocean. Atmos. Admin., College Park, Md.
Wang, H., J. Zhu, and J. Yang (2014), Error analysis on ESA's Envisat ASAR wave mode significant wave height retrievals using triple collocation model, *Remote Sens.*, *6*, 12,217–12,233.
Young, I. R., S. Zieger, and A. V. Babanin (2011), Global trends in wind speed and wave height, *Science*, *332*, 451–455.
Young, I. R., A. V. Babanin, and S. Zieger (2013), The decay rate of ocean swell observed by altimeter, *J. Phys. Oceanogr.*, *43*, 2322–2333.
Zieger, S., A. V. Babanina, W. E. Rogersb, and I. R. Young (2015), Observation-based source terms in the third-generation wave model WAVEWATCH, *Ocean Modell.*, *96*, 2–25.